Predictability of Mesoscale Rainfall in the Tropics

SHAFIQUL ISLAM*

Department of Civil and Environmental Engineering, University of Cincinnati, Cincinnati, Ohio

RAFAEL L. BRAS

Ralph M. Parsons Laboratory, Massachusetts Institute of Technology, Cambridge, Massachusetts

KERRY A. EMANUEL

Department of Earth, Atmosphere, and Planetary Sciences, Massachusetts Institute of Technology, Cambridge, Massachusetts

ABSTRACT

A general framework has been developed to study the predictability of space–time averages of mesoscale rainfall in the tropics. A comparative ratio between the natural variability of the rainfall process and the prediction error is used to define the predictability range. The predictability of the spatial distribution of precipitation is quantified by the cross correlation between the control and the perturbed rainfall fields. An upper limit of prediction error, called normalized variability, has been derived as a function of space–time averaging. Irrespective of the type and amplitude of perturbations, a space–time averaging set of 25 km^2–15 min (or larger time averaging) is found to be necessary to limit the error growth up to or below the prescribed large-scale mean rainfall.

1. Introduction

The lack of periodicity in atmospheric dynamics and the nonlinear coupling of its variables places an upper bound on our ability to forecast. Nonlinear equations, even with low dimensionality, exhibit sensitive dependence on initial conditions (SIC). Therefore, long-term predictability of the atmosphere is limited even though its deterministic description may be possible. Additional complexities arise in the atmosphere because of the interactions of physical–dynamical processes operating on a variety of space and time scales.

There is a wide spectrum of variation in range of predictability with scales. On one end, high-frequency fluctuations in point rainfall makes it highly unpredictable, whereas on the other end, daily average precipitation integrated over the tropics is almost equal to the surface evaporation and hence "perfectly" predictable. In hydrologic applications, for example, flash-flood forecasting, we are interested in predicting the spatial and temporal variability of storm rainfall at a

scale somewhere in between these two extremes. The spatial scales of interest in hydrology range from few to several thousand square kilometers, whereas temporal scales of prediction vary between a few minutes to several hours. This paper will investigate the range of predictability of rainfall at these scales. It is based on two fundamental hypotheses:

1) the physical laws that govern the behavior of atmosphere are well represented by an atmospheric model where the governing equations are deterministic and known; and

2) inherent instability of the atmosphere places an upper bound on the predictability of hydrometeorological quantities, and this bound can be approximated by estimating the divergence of "identical-twin" solutions of the model that differ slightly in their initializations.

Taken at face value, the first hypothesis implies that given the "exact" present state of the atmosphere (in the model), we can forecast the future states perfectly. The governing equations, however, that describe the physical–dynamic processes underlying precipitation form a highly nonlinear deterministic system. Even in some of the apparently simple mathematical models, nonlinearity coupled with sensitive dependence on initial conditions produces outputs indistinguishable, by standard techniques, from a stochastic process.

---

* Formerly at Ralph M. Parsons Laboratory, Massachusetts Institute of Technology, Cambridge, Massachusetts.

Corresponding author address: Rafael L. Bras, Ralph M. Parsons Laboratory, Department of Civil Engineering, Building 48-305, MIT, Cambridge, MA 02139.

The lack of complete periodicity in the atmosphere's behavior supports the second hypothesis; however, it does not reveal the range at which the prediction error becomes unacceptably large. To study the range of predictability, we will concentrate on the divergence of "identical-twin" solutions of governing equations that differ only in their initializations. The rate at which twin solutions of the model diverge shows how rapidly initial small errors will grow to make the prediction useless. It is likely that point rainfall will diverge very quickly, rendering a predictability range of a few minutes at the most, whereas domain-averaged rainfall will most probably converge for the twin solutions, implying a perfect predictability. A logical question to ask at this point is: How does the range of predictability vary as a function of temporal and spatial averaging? The answer to such a question will aid significantly in using physically based mesoscale models for extensive predictive applications like flood predictions. Operationally, to name a few, these results can be used to design the optimal set of space–time averaging for remote sensors and to determine the resolution of flood-forecasting models for a given predictability range.

Since Lorenz' (1965) pioneering work on predictability of the atmosphere with a low-order baroclinic model, several error-growth studies have been performed with ever increasing complex models of the atmosphere (for example, Charney et al. 1966; Leith 1965; Lorenz 1982; Mintz 1964; Smagorinsky 1969; Shukla 1981). All these experiments attempted to characterize the error growth of extended-range forecasts for large-scale atmospheric flows. Based on some of these large-scale predictability studies and homogeneous turbulence theory, pessimistic conclusions were drawn concerning mesoscale predictability (Tennekes 1978). Several counterarguments were also made to suggest that prediction of some important mesoscale phenomena is far more encouraging than the preceding conclusions indicate (Anthes et al. 1985).

In recent years, considerable effort has been put into the development and testing of mesoscale models. Yet compared to predictability of large-scale systems, very little attention has been directed toward quantifying predictability of mesoscale weather systems. Limited-area predictability studies are not a straightforward extension of the global-scale studies. The mesoscale weather differs from synoptic–planetary systems in many ways; for example, in their time scales, intermittencies, and triggering mechanisms. In addition, added complexity is introduced due to the presence of lateral boundary conditions (LBC) in mesoscale models. Errors introduced by the LBC, which are not present in global models, contribute additional errors to the predictions (Baumhefner and Perkey 1982). On the other hand, in certain synoptic situations, LBC may supply useful information and may help in increasing the predictability range.

Anthes et al. (1985) utilized a three-dimensional, primitive equation model to estimate the predictability of meso-α-scale (200–2000 km) motions in a regime characterized by organized moist convection. They looked at error growth of instantaneous values of several variables but never looked at rainfall. Surprisingly, this study showed little or no growth of rms errors due to the error in specifying initial conditions over the time period of 0–72 h. In contrast, the simulations were more sensitive to the specification of lateral boundary conditions. The reasons for the differences in predictability behavior between large-scale models and this study are not clear. Anthes et al. (1985) hypothesized that nearly identical LBC imply that larger horizontal scales information is also nearly identical and this feature, coupled with fixed model fields such as topography, almost exclusively determine the smaller-scale behavior. Consequently, perturbations in initial conditions have almost no effect on the growth of rms error. In addition, Anthes et al. (1985) introduced their perturbation in such a way that the slower modes are affected most. This scale-selective perturbation procedure may also be responsible for the increased predictability.

A different analysis by Errico and Baumhefner (1987), using a high-resolution limited-area model, indicated that coupling of several model properties is responsible for restricted error growth. Typically, a major portion of the initial perturbation is either dissipated by numerical filters or diabatic processes or is propagated out of the forecast domain due to its projection onto gravity waves. At small scales, parameterized horizontal diffusion is found to be very effective at dissipating errors. In contrast with errors, the fields themselves do not weaken in time, which implies a substantial forcing of small scales by large scales.

Of course, these conclusions are not likely to be applicable to other mesoscales (e.g., meso-β scales ranging from 20 to 200 km or meso-γ scales ranging from 2 to 20 km) where various instabilities may influence a significant portion of the model domain. At hydrologic scales (which may be compared to the meso-β scale but without implying that the hydrologic scales are independent of either meso-α or meso-γ scales), we expect considerably more divergence of solutions due to the variation in initial conditions. It is worthwhile to mention that no systematic predictability studies have been reported at these scales to date.

2. Design of the experiment

One major impediment to testing any hypothesis regarding predictability is the quality and quantity of observational data. This scarcity of data is particularly true at spatial scales that are comparable to the hydrologic prediction scales themselves. As previously implied, our analysis will be based on a limited-area, three-

dimensional numerical cloud model developed by Clark (1977, 1979) and his collaborators (e.g., Clark and Hall 1979; Clark and Farley 1984; Smolarkiewicz and Clark 1986). Of course, results and conclusions based on simulated data are valid only to the extent that the assumptions and approximations of the cloud model are valid.

Our approach in creating the model atmosphere for predictability studies will be somewhat different from most of the previous simulation experiments with limited-area models. Conventionally, cumulus convection simulations start with a large reservoir of convective available potential energy and are not forced. Consequently, the results based on these type of experiments have a strong dependence on the choice of the initial sounding. An attempt is made to eliminate this dependence by creating a model atmosphere that is in radiative–convective equilibrium. Our predictability experiments will be performed after this equilibrium state has been reached.

As a mechanism to create the equilibrium situation, we will assume that surface heat flux is in balance with radiative cooling of the troposphere. This way no net heat will be put into the model domain. Since our simulation time (in the range of several hours) will be much smaller than the time scale over which large-scale forcing changes, it is expected that this representation of uniform forcing will be adequate.

Our region of interest is the tropics. The model domain is 3600 km^2 (60 km $\times$ 60 km) and 20 km deep, with a horizontal resolution of 2 km and a vertical resolution of 250 m. Cyclic boundary conditions are used in the horizontal, while the top and bottom boundaries are fixed; however, to avoid the reflection of gravity waves from the model top, a 5-km-deep Rayleigh friction absorber is employed at the top. A more detailed description of the experiment may be found elsewhere (Islam 1991).

Horizontally homogeneous heat and moisture fluxes are added to the atmosphere from the surface and at the same time radiative cooling is applied up to the tropopause. The balance between the surface fluxes and radiative cooling is imposed to guarantee that the model atmosphere evolves into an equilibrium state. A simple perturbation of sensible heat flux Q_S is used to create the initial field of motion. The intensity of the perturbation is increased progressively to reach a maximum amplitude of 10% of Q_S at 30 min. The perturbation is terminated at 30 min, and thereafter the surface heat fluxes remain horizontally homogeneous. A horizontally homogeneous Bowen ratio ($B = Q_S/Q_L$) of 0.50 is assumed, where Q_L is the latent heat flux. This type of partitioning between sensible and latent heat fluxes is reasonable for large wetlands. Therefore, given the sensible heat flux at a point, we can easily get the latent heat flux. The changes in temperature T and water vapor mixing ratio q_v of a layer

of thickness Δz just above the lower surface of the model are

$$\frac{\partial T}{\partial t} = \frac{Q_S}{C_p \rho \, \Delta z}, \qquad (2.1)$$

$$\frac{\partial q_v}{\partial t} = \frac{Q_L}{L_v \rho \, \Delta z}, \qquad (2.2)$$

where C_p, ρ, and L_v are the specific heat, density of air, and latent heat of vaporization, respectively. Surface heat fluxes of 166 W m^{-2} (Q_S) and 332 W m^{-2} (Q_L) produce a rate of temperature change of $1.95°C$ h^{-1}, and a rate of change in mixing ratio of 1.56 g kg^{-1} h^{-1} at the surface grid points (if $\Delta z = 250$ m). To compensate for the surface heat flux, we need to provide a uniform radiative cooling at the rate of 6°C day^{-1} uniformly from the surface up to the tropopause (13 km). The chosen values of surface fluxes and radiative cooling are somewhat larger than the typically observed ones; they are chosen to enhance the approach to equilibrium. Nevertheless, large-scale mean ascent in the tropics at times may produce an adiabatic cooling several times larger than the typical radiative cooling of 2°C day^{-1}. Since the current model formulation cannot explicitly account for the large-scale ascent, an attempt will be made to incorporate this effect by choosing a larger value for the radiative cooling.

Our interest lies in creating a model atmosphere that is in a state of statistical equilibrium; hence, the initial sounding should not be important in deciding the final outcome of the predictability experiment. The mean soundings for the West Indies area (Jordan 1958) are used for this purpose.

3. Predictability experiment

To study the errors in prediction, our focus will be on the divergence of a control run and a perturbed run, with the perturbation occurring after equilibrium state has been reached. What follows is the definition of the equilibrium state and the details of the perturbation.

a. Definition of equilibrium

Since the route to the equilibrium state is controlled by the chosen balance of surface heating and radiative cooling, it is reasonable to expect that, in equilibrium, a moving average of rainfall intensity should be close to the surface evaporation rate. However, it is evident from the time history of domain-averaged rainfall intensity (Fig. 1a) that the individual fluctuations of the rainfall intensity around the evaporation rate can be large. Therefore, an objective way to define the equilibrium state needs to be found. We will assume that the rainfall has reached equilibrium if the second-order statistics of domain-average rainfall stabilize with time.
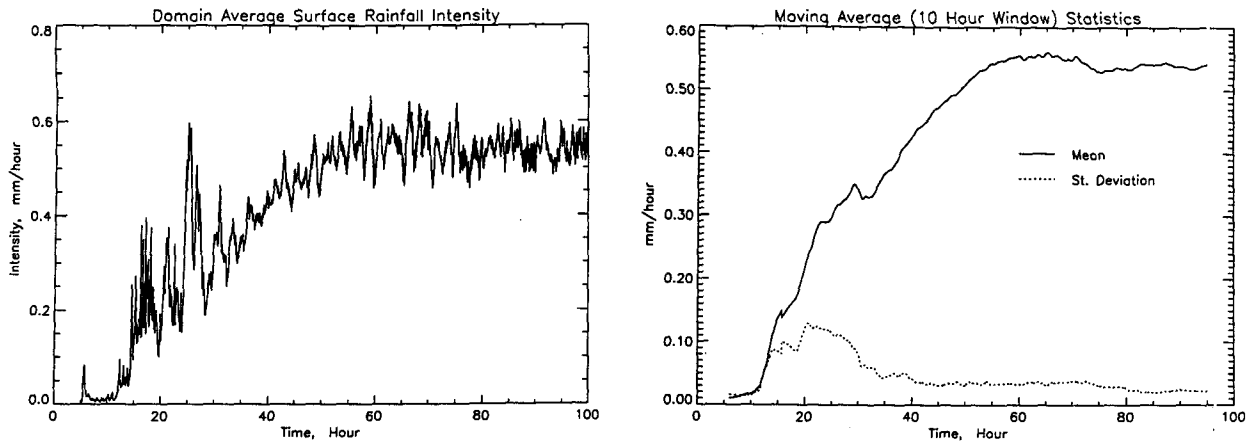
FIG. 1. (a) Domain-average surface rainfall intensity. (b) Moving-average statistics for the domain average surface rainfall intensity.

Figure 1b shows the moving average mean and standard deviation with a 10-h averaging window. As can be seen, the domain-averaged rainfall starts out low and gradually increases and fluctuates around the large-scale evaporative flux, the moving average mean shows an increasing trend up to 50 h and then remains essentially constant, and the standard deviation stabilizes at about 40 h. Based on these observations, it is argued that the rainfall process has reached an equilibrium state after 50 h. This state, in principle, is independent of the initial sounding.

Now look at the space–time evolution of three other variables, namely, potential temperature, relative humidity, and cloud water, to ensure that the model atmosphere has indeed reached equilibrium. Figure 1c shows the horizontally averaged potential temperature field along with the associated root-mean-square (rms) deviation at 20, 40, 50, and 60 h. The average profile at 20 h is slightly warmer than that at 40 h. The profiles at 50 and 60 h are virtually indistinguishable. Another point to notice is that the rms deviation decreases up to the tropopause as the equilibrium condition is approached. Relatively higher rms deviation above the tropopause may result due to the presence of 5-km-deep Rayleigh friction absorber at the top and possibly due to the excited internal waves. Figure 1d shows the horizontally averaged relative humidity profile and the associated rms deviation. From 40 h onward, the profiles do not seem to change with time. Although these are instantaneous values, they clearly show that the model has reached equilibrium after 50 h. A curious feature to note is the presence of nearly saturated layer between 8 and 14 km. This high-tropospheric relative humidity suggests that the entire layer is saturated and filled with cloud. Figure 1e shows three-dimensional views of the cloud-water field exceeding 0.50 gm kg^{-1} at 20, 40, 50, and 60 h. The cloud-water field at 20 h looks realistic; however, as time progresses, the layer between 8 and 14 km keeps building up cloud-water

content. This may be an artifact of the Kessler warm-rain parameterization. In the parameterization, for the autoconversion of cloud water to rainwater to occur, the cloud water should exceed a certain threshold. That threshold is taken to be 0.50 gm kg^{-1}. In addition, there is a rate of conversion that is used as 10^{-3} s^{-1}. As the simulation time increases, more and more cloud water gets deposited at these levels essentially due to the Kessler scheme having an effective bypass filter effect. This deck of cloud should not have any significant effect on the dynamics of our simulations, however, because of the specified radiative cooling. If an interactive radiative scheme was used, this could lead to a runaway solution.

It seems that starting our predictability studies from this equilibrium may prove illuminating in at least two ways. First, this construction of equilibrium model state is physically and thermodynamically close to the observed atmosphere (Xu and Emanuel 1989; Betts 1982); hence, the model is more likely to mimic the interaction of real cumulus clouds with the real atmosphere and consequently will be able to produce physically meaningful results. Second, predictability experiments with this type of model state have never been pursued and may yield a very different predictability range.

b. Introduction of perturbations

Following the above definition, the potential temperature field is perturbed well within the equilibrium regime at 60 h. The amplitude of the perturbation is chosen to be uniformly distributed within the interval −0.25 to 0.25 K. To eliminate any spatial bias, this form of zero mean perturbation is introduced at all the horizontal and vertical nodes. It should be noted here that the amplitude of the perturbations is within the instrumental accuracy of temperature measurement in the atmosphere. The control and perturbed
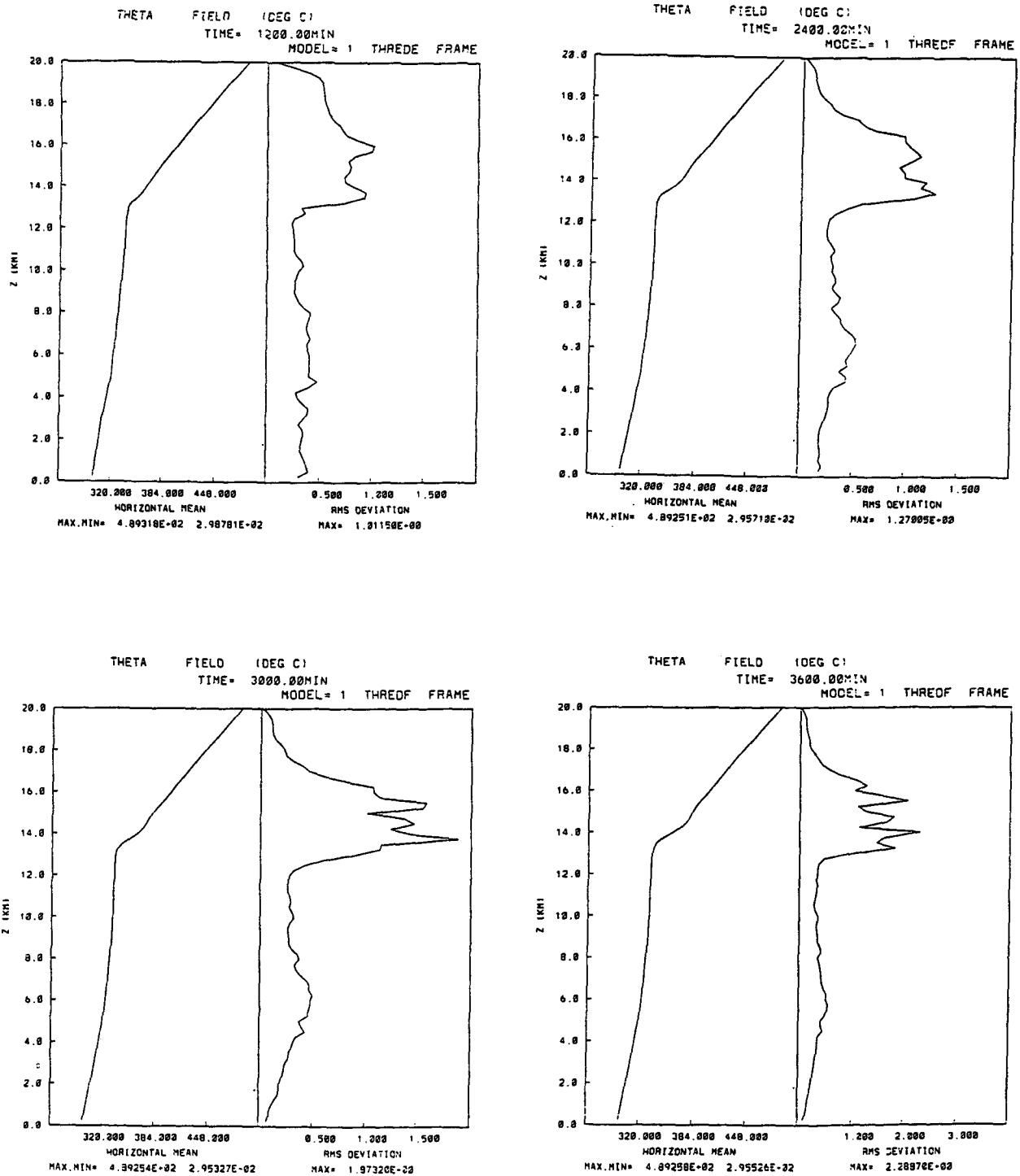
FIG. 1c. Horizontally average potential temperature profiles with associated root-mean-square deviation at 20, 40, 50, and 60 h.

experiments are then run for 20 h (i.e., from 60 to 80 h). Comparisons of these two simulations will yield the range of predictability.

Figure 2a shows the time history of domain-averaged rainfall for both the runs. Although these are domain-averaged quantities, the temporal fluctuations of rain-
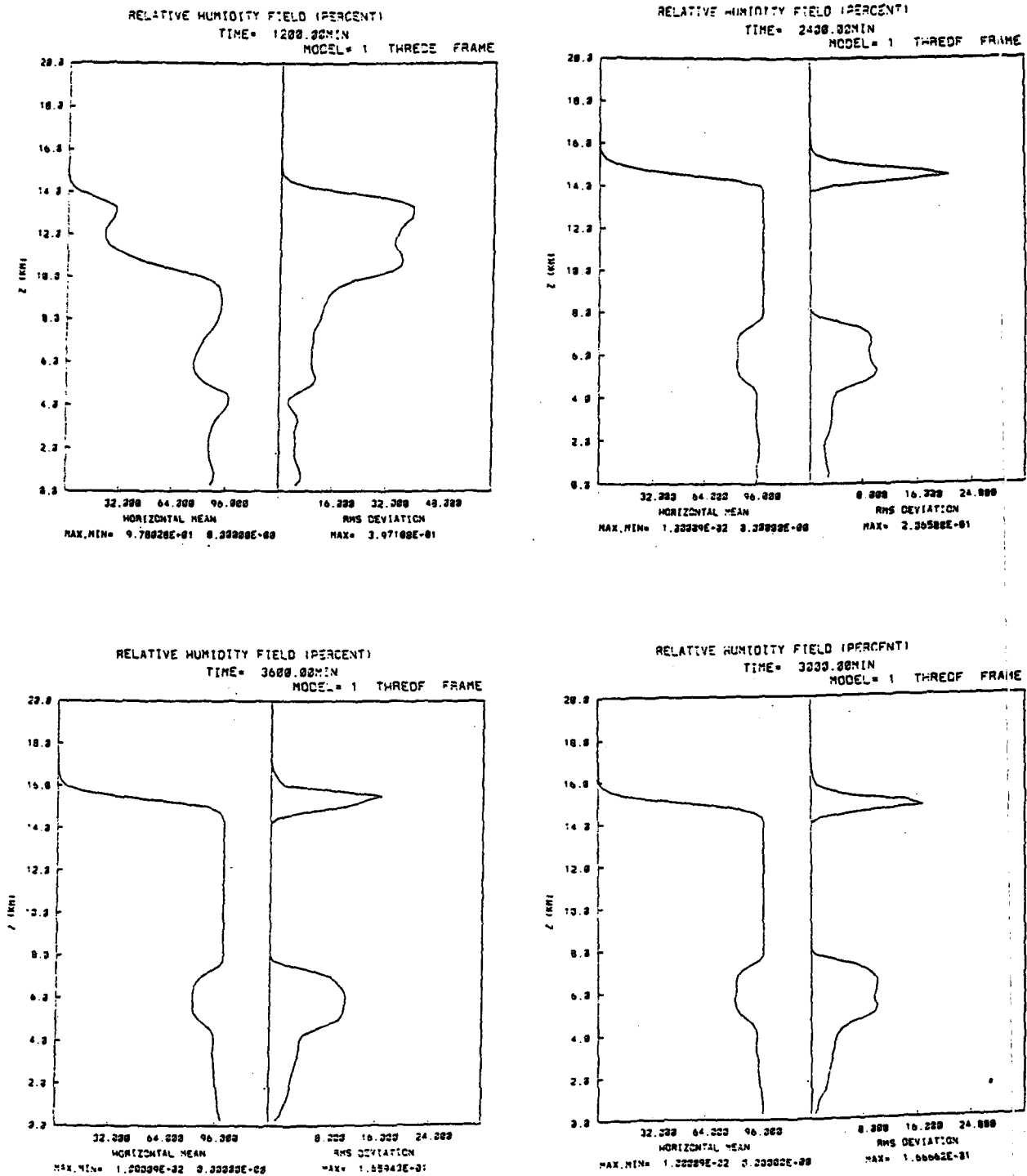
FIG. 1d. Similar to Fig. 1c but for relative humidity.

fall intensity are large. Figures 2b,c show the spatial distribution of surface rainfall intensity for both the control and the perturbed run at selected times. Although the simulations are performed at 10-s time steps, these plots show rainfall intensity averaged over 15 min. The simulations satisfactorily mimic the observed spatial pattern of convective rainfall in both the cases. For the first hour, the two solutions are almost

VALUES.GE. 0.5000E-00 AT TIME= 1200.00MIN
QC FIELD (GR/KG)

VALUES.GE. 0.5000E-00 AT TIME= 2400.00MIN
QC FIELD (GR/KG)

VALUES.GE. 0.5000E+00 AT TIME= 3000.00MIN
QC FIELD (GR/KG)

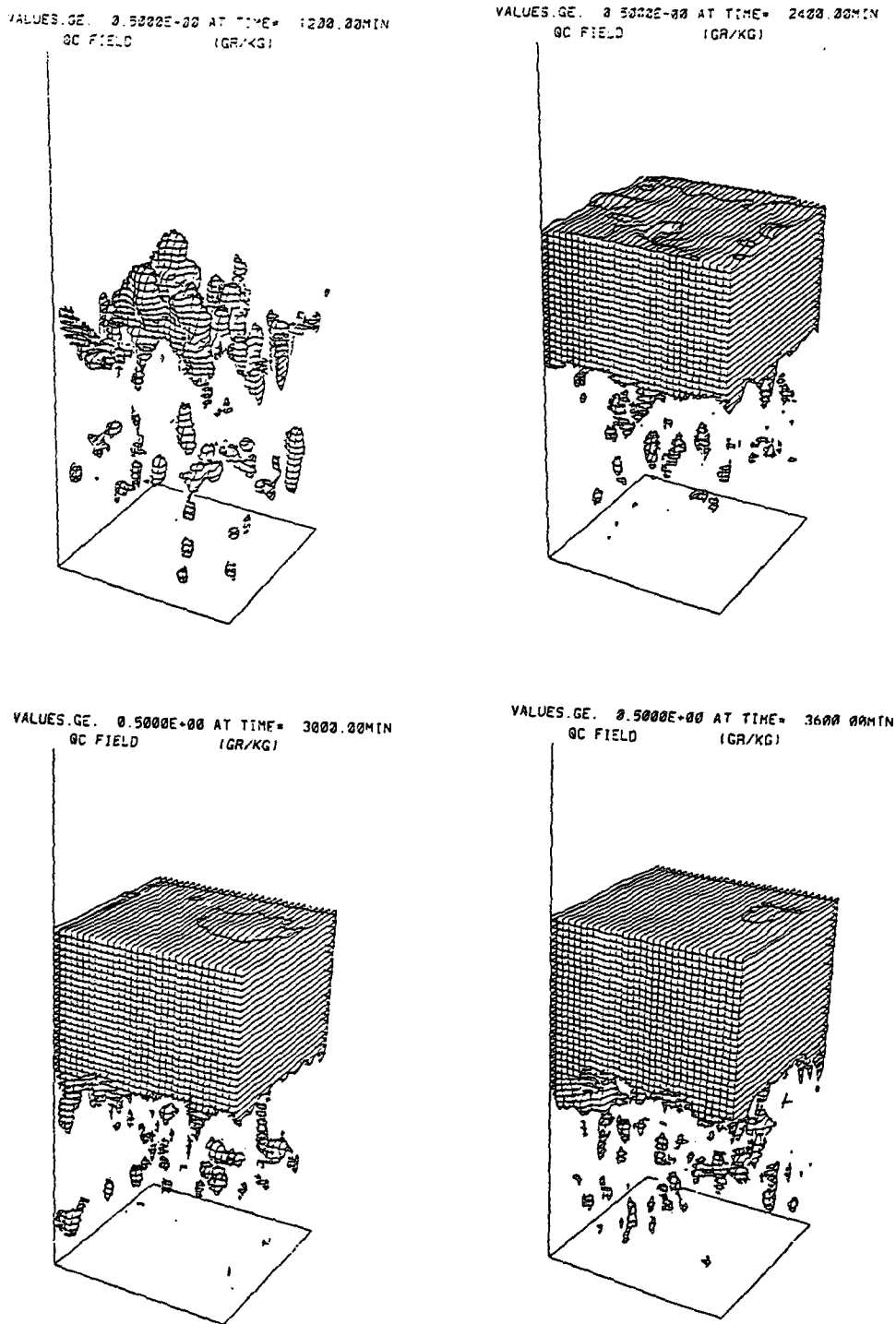VALUES.GE. 0.5000E+00 AT TIME= 3600 00MIN
QC FIELD (GR/KG)

FIG. 1e. Three-dimensional cloud-water field at 20, 40, 50, and 60 h.

indistinguishable from each other. However, gradually they drift apart and become totally uncorrelated. Figures 2d,e show the spatial structure of the absolute pre- diction error. For the first hour, there is virtually no error; however, as the prediction time increases, more and more spatial disparity appears.
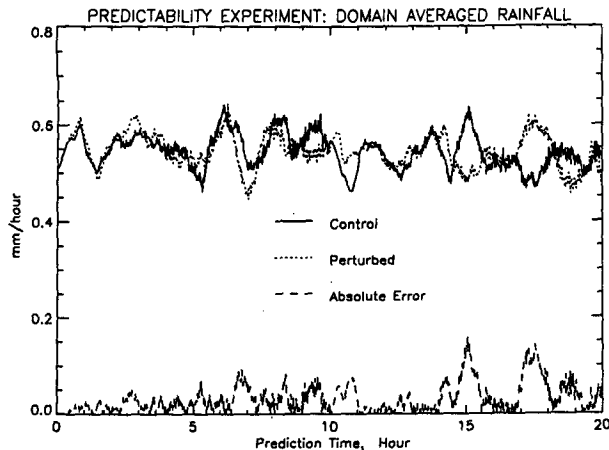
FIG. 2a. Domain-average surface rainfall intensity for the control and the perturbed simulations along with the absolute prediction error.

4. Measures of predictability time

For hydrometeorological applications, knowledge about both temporal and spatial structure of rainfall is of importance. Therefore, a suitable predictability measure should include temporal variability as well as spatial nonhomogeneity. For large-scale atmospheric predictability studies, usually the doubling time of "small" initial errors is taken as a measure of predictability range. To use this measure, several assumptions have to be invoked to quantify the initial error as small; in addition, this is a spatially averaged measure and does not give any information about the spatial aspects of predictability.

Warner and Keyser (1983) looked at several characteristic features of mesoscale predictability and proposed a useful definition that states:

> "Given a perfectly predictable large scale atmospheric structure, a measure of mesoscale predictability is the time required for a specified error in the mesoscale structure of one or more variables to cause the prediction of a specific quantity to be sufficiently in error so that it has essentially zero utility."

This definition measures predictability in terms of a time scale, but it does not account for the skill embodied by a prediction prior to the time when it had zero utility. Also, the rather vaguely used term "zero utility" needs a rigorous definition. On the other hand, this definition clearly recognizes the predictability implications of scale interactions. In our proposed measure of predictability time, this definition will be used as a basis. However, the term "zero utility" will be temporally quantified by comparing the prediction error with the perfectly known large-scale mean rainfall and spatially by choosing a level of correlation between the control and the perturbed field.

The use of a comparative difference between the natural variability of the rainfall process and the prediction error as a measure of predictability in time is proposed. This measure explicitly recognizes the fact that there is an inherent variability in the rainfall process. In space, the cross correlation between the control and perturbed rainfall field at an instant will be used. Then a time history of cross correlation will yield a predictability range for a chosen level of correlation.

a. Temporal measure

First the loss of information is quantified as a function of time elapsed since the perturbation. This will be a measure of predictability in time. Define the spatially averaged prediction error $E^{mn}(t)$ as

$$E^{mn}(t) = \left\{ \frac{1}{N_x N_y} \sum_{i=1}^{N_x} \sum_{j=1}^{N_y} [C_{i,j}^{mn}(t) - P_{i,j}^{mn}(t)]^2 \right\}^{1/2},$$

$$(4.1)$$

where $C_{i,j}^{mn}(t)$ and $P_{i,j}^{mn}(t)$ are the control (or observed) and perturbed rainfall process at a spatial location (i, j) for a specific level of temporal and spatial averaging, m and n. Parameters N_x and N_y are the number of grid points in x and y directions, respectively; these will change with the level of spatial average n. For example, for $n = 2$ km, we have $N_x = N_y = 30$; whereas for $n = 10$ km, we only have $N_x = N_y = 6$. For now, the focus will be on spatial averaging in terms of square boxes of side n; an extension to rectangular or other geometric shapes is rather straightforward.

As a measure of natural variability of the process, the standard deviation of the control rainfall σ_c^{mn} will be used as a function of space–time averaging:

$$\sigma_c^{mn} = \left[\frac{1}{N_x N_y N_t} \sum_{k=1}^{N_t} \sum_{i=1}^{N_x} \sum_{j=1}^{N_y} (C_{i,j,k}^{mn} - \bar{C})^2 \right]^{1/2}, \quad (4.2)$$

where subscript k denotes time and N_t is the total number of time steps. The rainfall-process statistics are estimated using a 50-h period (between 50 and 100 h) from the onset of the equilibrium regime. A 10-s time step is used for the simulations, which implies that 16 200 000 space–time pairs are given to estimate the process statistics. Notice that the mean $\bar{C}$ is not affected by the averaging operator. In the limit, for sufficiently large space–time averages, $\bar{C}$ should approach the large-scale evaporative flux. In our case, the difference in total rainfall (defined as the 20-h cumulative rainfall for the entire domain) for the control and the perturbed run is less than 5%.

Figures 3a–d show the ratio of spatially averaged prediction error and the process standard deviation as a function of the prediction time for a variety of space–time averages. In all the cases, the normalized prediction error grows with time and eventually approaches and fluctuates about $\sqrt{2}$.
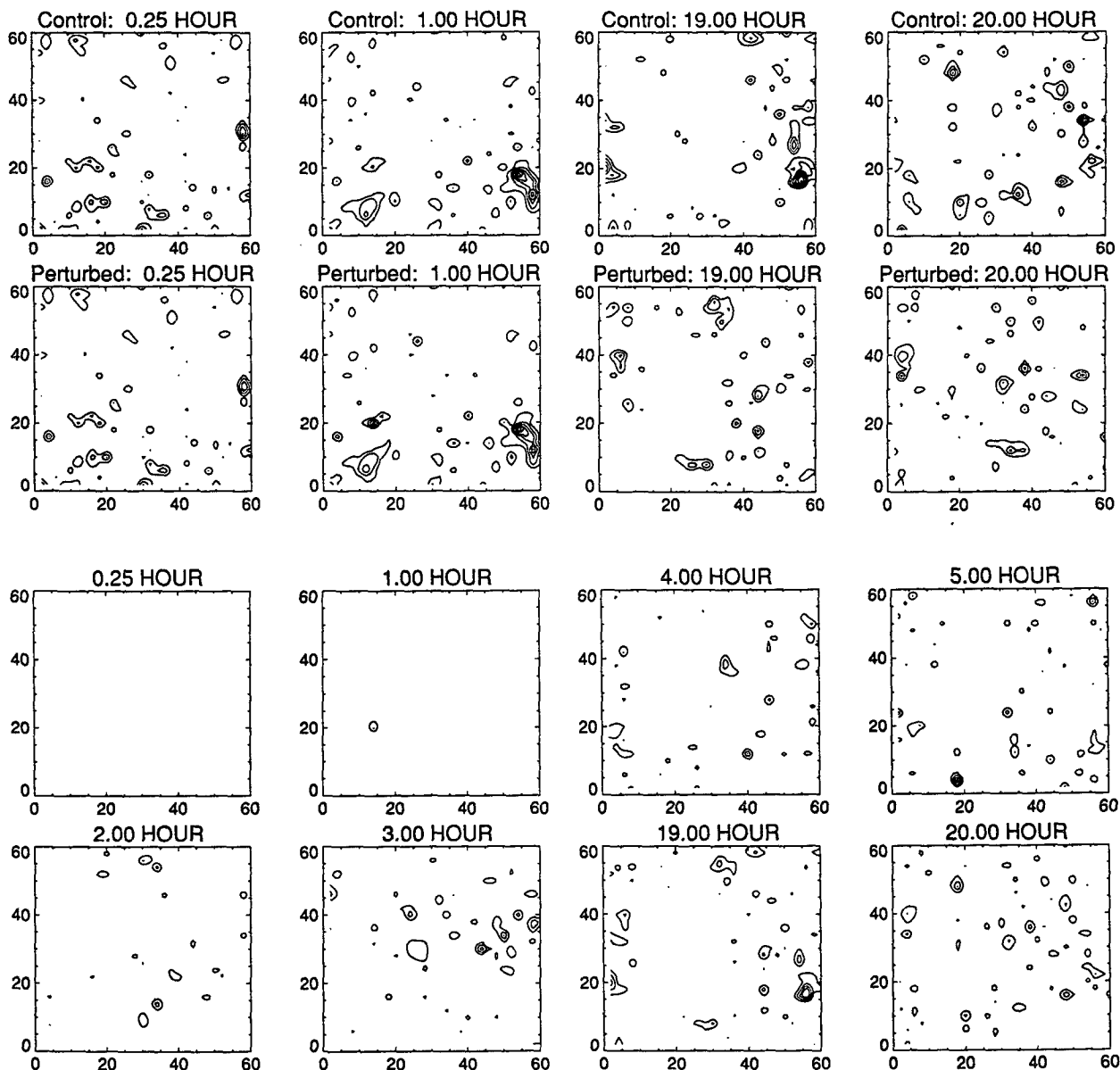
FIG. 2. (b) Spatial distribution of rainfall intensity for the control and the perturbed experiments at 15 min and 1 h. (c) Similar to (b) but for 19 and 20 h. (d) Spatial distribution of the absolute prediction error for selected times. (e) Similar to (d).

This limiting value can be derived. Assume that the mean $\bar{C} = \bar{P}$, and the standard deviations, $\sigma_c^{mn} = \sigma_p^{mn}$, of the control and the perturbed process are the same. Since both processes are controlled by the same dynamics and physics, this assumption is exactly true for $t \to \infty$ and large spatial domain. For notational simplicity, omit m, n, and t from (4.1), although keep in mind that the subsequent analysis is valid for large t. In addition, if we assume that the spatial average corresponds to the ensemble average, then we can write

$$E^2 = \langle (C - P)^2 \rangle \qquad (4.3)$$

where $\langle \ \rangle$ refers to the ensemble average. Now if (4.3) is expanded and the control and the perturbed process are treated as independent, which is a fair assumption for large t, it can easily be shown that

$$E^2 = 2\sigma_C^2 \quad \text{i.e.,} \quad \frac{E}{\sigma_c} = \sqrt{2}. \qquad (4.4)$$

It is interesting to notice that the spatially averaged error attains the same asymptotic limit for a variety of space–time averages.
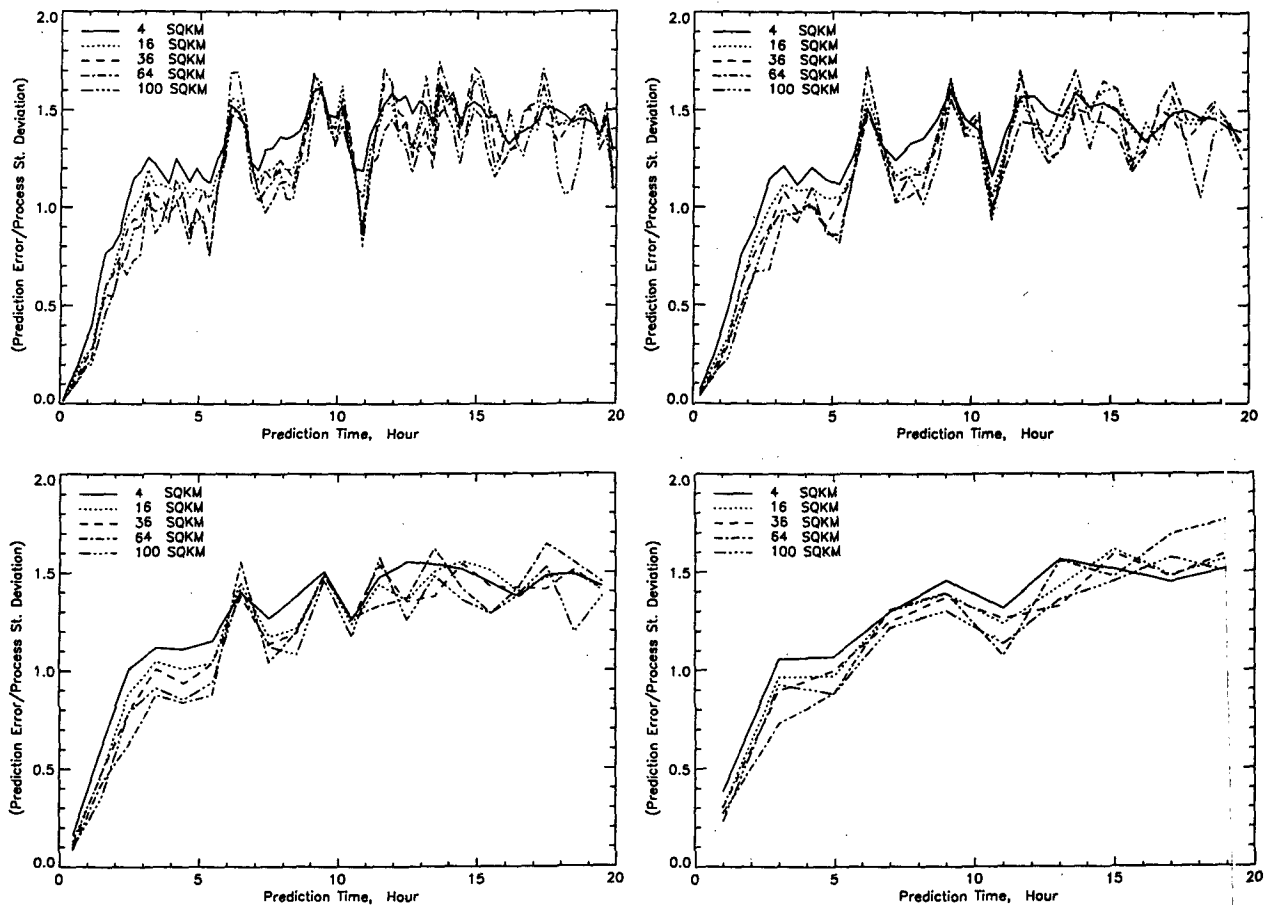
FIG. 3. (a) Spatially averaged prediction error for 15-min averages. (b) Similar to (a) but for 30-min averages. (c) Similar to (a) but for 1-h averages. (d) Similar to (a) but for 2-h averages.

Given the perfect knowledge of large-scale atmospheric forcing, a useful measure of predictability range is the time required for the prediction error to reach a certain fraction of the known large-scale mean rainfall, that is,

$$T^{mn} : E^{mn}(t) \leqslant \alpha \bar{C}, \qquad (4.5)$$

where T^{mn} is the predictability time for a specific level of space–time smoothing, and α is an arbitrary constant that will quantify how stringent one is in estimating predictability time. For example, for $\alpha = 0.10$, we demand a tenfold higher accuracy in prediction compared with $\alpha = 1.0$. This may be thought as a "risk factor" associated with a particular decision when these results will be used.

Given the limiting result of (4.4), an upper limit of prediction error can be specified as a function of space–time averaging without even performing the perturbation experiment. If normalized variability, defined as $\sqrt{2}\,\sigma_c^{mn}/\bar{C}$, is plotted in an m–n space (Fig. 4), then, given a desired level of accuracy of prediction, we can infer the required size of the space–time averaging box.

In other words, normalized variability refers to the percentage departure of the saturation prediction error from the known large-scale mean rainfall. A normal-
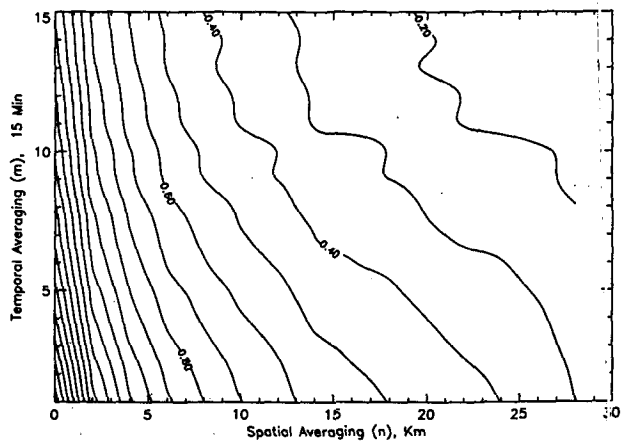

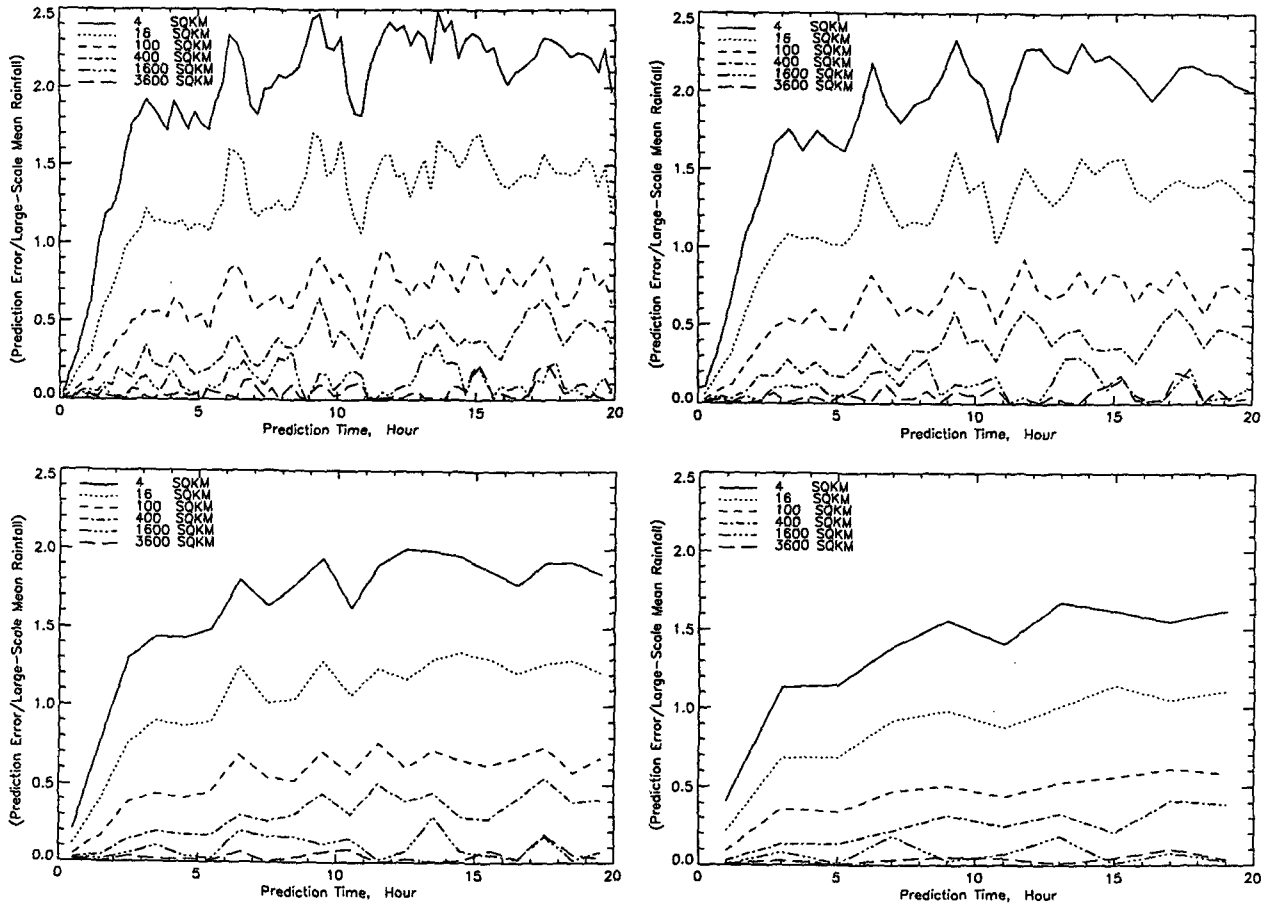FIG. 4. Normalized variability as a function of space–time averaging.

FIG. 5. (a) Spatially average prediction error for 15-min averages. (b) Similar to (a) but for 30-min averages. (c) Similar to (a) but for 1-h averages. (d) Similar to (a) but for 2-h averages.

ized variability of zero implies perfect predictability, which is the limiting result for large m and n. As the size of the space–time averaging box increases, the difference between the large-scale prescribed mean and the predicted mean decreases and eventually becomes zero. The averaging set m and n, corresponding to the normalized variability of unity, will make a prediction error as large as the large-scale mean. The prediction time when such an error is incurred will depend on the size of m and n. The steep slopes of the contours to the left of the unit contour imply that in this region temporal averaging as large as 4 h will not have much effect in increasing the predictability time. On the other hand, the averaging sets falling to the right will never incur an error as large as the known mean.

Figures 5a–d show the temporal evolution of the prediction error normalized by the large-scale mean as a function of space–time averaging for a given amplitude of perturbation. As expected, with increasing m and n, the prediction error decreases. These figures can be used to exactly determine T^{mn} for a given value of m, n, and α.

b. Spatial measure

To quantify the predictability of the spatial distribution of precipitation, the correlation between the control and the perturbed rainfall field $\rho_{cp}^{mn}(t)$, will be used as a function of prediction time:

$$\rho_{cp}^{mn}(t) = \varphi(t) \sum_{i=1}^{N_x} \sum_{j=1}^{N_y} [C_{i,j}^{mn}(t) - \bar{C}(t)]$$

$$\times [P_{i,j}^{mn}(t) - \bar{P}(t)], \quad (4.6)$$

where

$$\varphi(t) = \{N_x N_y [\sigma_c^{mn}(t)][\sigma_p^{mn}(t)]\}^{-1},$$

$$\bar{C}(t) = \frac{1}{N_x N_y} \sum_{i=1}^{N_x} \sum_{j=1}^{N_y} C_{ij}(t),$$

$$\sigma_c^{mn}(t) = \left\{\frac{1}{N_x N_y} \sum_{i=1}^{N_y} \sum_{j=1}^{N_x} [C_{ij}(t) - \bar{C}(t)]\right\}^{1/2}, \quad \text{and}$$

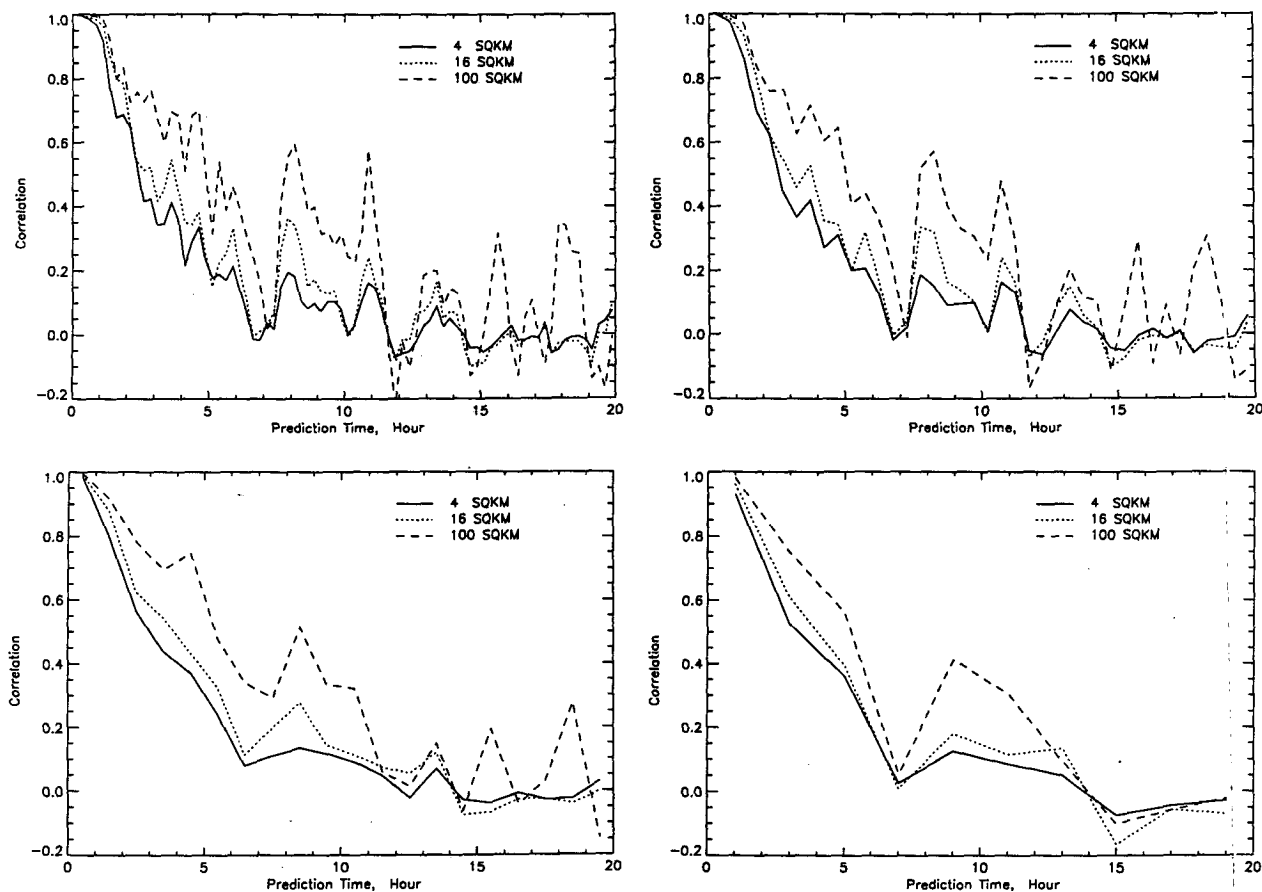σ_p^{mn} is defined similarly to σ_c^{mn}.

FIG. 6. (a) Correlation between the control and the perturbed rainfall field for 15-min averages. (b) Similar to (a) but for 30-min averages. (c) Similar to (a) but for 1-h averages. (d) Similar to (a) but for 2-h averages.

Following the arguments and assumptions of the previous section and omitting m, and n, and t for notational simplicity, we can write

$$\rho_{cp} = \frac{\langle (C - \bar{C})(P - \bar{P}) \rangle}{\sigma_c \sigma_p}. \qquad (4.7)$$

Expanding (4.7) gives

$$\rho_{cp} = \frac{\langle CP \rangle - \bar{C}\bar{P}}{\sigma_c \sigma_p}.$$

For large t, if C and P are assumed to be independent, then ρ_{cp} becomes zero. This time of zero correlation may serve as a criterion for estimating predictability time. This may not be a very useful criterion because zero correlation essentially means that the control and the perturbed field are two realizations of a random process. A more flexible and meaningful criterion for estimating predictability time may be defined as

$$T^{mn} : \rho_{cp}^{mn}(t) \geqslant \beta, \qquad (4.8)$$

where β is an arbitrary constant between 0 and 1.0. Although the correlation may take a negative value, negative correlation does not have any useful meaning in the context of predictability time. Figures 6a–d show the spatial correlation as a function of prediction time for several levels of space–time smoothing. Given these figures and a chosen level of correlation β, T^{mn} can be estimated graphically. An interesting feature to notice in all these figures is that for different combinations of m and n, the correlation appears to be positive for almost all the time. The implication is that at a given time, on the average, the number of spatial locations overestimating (or underestimating) the mean is equal in both the control and the perturbed run.

5. Concluding remarks

Compared with large-scale atmospheric systems, the efforts to quantify predictability of mesoscale systems have been very limited. In this paper, we have developed a general framework to study the predictability

of space–time averages for mesoscale rainfall in the tropics. In the following two subsections, we will summarize and highlight the important conclusions.

a. Equilibrium experiment

We have created an equilibrium model atmosphere by requiring a balance between the surface heat fluxes and radiative cooling. For the given forcing, it takes about 50 h to reach a radiative–convective equilibrium. At equilibrium, the variability of the domain- (3600-km^2) average rainfall is small, suggesting that the predictability will increase with space–time averaging. In addition, 3600 km^2 is small compared to the space scale of cyclones. This may imply that the convection will be in equilibrium with cyclonic-scale forcing. On the other hand, since the time required to reach equilibrium is of the order of cyclonic time scale, it is difficult to delineate the possible feedback between convective and cyclonic systems.

b. Predictability of space–time averages

In designing the predictability measures, we have emphasized both spatial and temporal variability of rainfall. We use a comparative difference between the natural variability of the rainfall process and the prediction error as a measure of predictability in time. In space, a chosen level of cross correlation between the control and the perturbed rainfall field defines the predictability range.

For a given forcing, an upper limit of prediction error, called normalized variability, has been derived as a function of space–time averaging. This limit is independent of the amplitude and spatial distribution of perturbations. The averaging space–time set corresponding to the normalized variability of unity implies that we will make a prediction error as large as the large-scale mean. The prediction time when such an error is incurred will depend on the averaging space–time set and the type of perturbation. Irrespective of the amplitude of perturbation, we find that a space–time averaging set of 25 km^2–15 min (or larger time averaging) is necessary to limit the growth of prediction error up to or below the large-scale mean.

Normalized predictability measures, both in space and time, have been developed for a set of perturbation amplitudes and shown in graphical form. The level of perturbations studied is comparable to instrumental errors in temperature measurements in the atmosphere. Hence, the perturbation experiments are illustrative of the propagation of errors in specifying initial conditions. The predictability measures and the given figures can be used to determine the predictability range for a given set of space–time averages with an associated risk factor and an amplitude of perturbation.

It should be emphasized that the conclusions are based on only one perturbation experiment and a restrictive nodal configuration. To extend the results, it is important to look at a reasonable ensemble of perturbation experiments, to simulate more realistic initial-error characteristics, and to quantify the sensitivities to surface forcing. In this context, several interesting questions may be posed for future research. The equilibrium state attained in the simulations is a function of the forcing. It is not clear how long it will take to reach the equilibrium condition with different forcing. Do we reach the same statistical equilibrium for different sets of forcing or do we get multiple equilibria for different forcing? Will the predictability change with spatially variable heat fluxes and radiative cooling? How do we modify Kessler parameterizations to get realistic cloud fields for longer periods of simulations? How does the result change if we use ice physics instead of warm-rain parameterizations? Can we put a confidence interval around our predictability estimates by choosing a family of perturbations?

REFERENCES

Anthes, R. A., Y. H. Kuo, D. P. Baumhefner, R. P. Errico, and T. W. Bettge, 1985: Predictability of mesoscale atmospheric motions. *Adv. Geophys.,* **28B,** 159–202.

Baumhefner, D. P., and D. J. Perkey, 1982: The relationship between present large scale forecast skill and new estimates of predictability error growth. *Predictability of Fluid Motions,* G. Holloway and B. J. West, Eds., American Institute of Physics, 169–180.

Betts, A. K., 1982: Saturation point analysis of moist convective overturning. *J. Atmos. Sci.,* **39,** 1484–1505.

Charney, J. G., R. G. Fleagle, H. Riehl, V. E. Lally, and D. Q. Wark, 1966: The feasibility of a global observation and analysis experiment. *Bull. Amer. Meteor. Soc.,* **47,** 200–220.

Clark, T. L., 1977: A small scale dynamic model using a terrain-following coordinate transformation. *J. Comp. Phys.,* **24,** 186–215.

——, 1979: Numerical simulations with a three-dimensional cloud model: Lateral boundary condition experiments and multicellular severe storm simulations. *J. Atmos. Sci.,* **36,** 2191–2215.

——, and W. D. Hall, 1979: A numerical experiment on stochastic condensation theory. *J. Atmos. Sci.,* **36,** 470–483.

——, and W. R. Farley, 1984: Severe downslope windstorm calculations in two- and three-spatial dimensions using anelastic interactive grid nesting: A possible mechanism for gustiness. *J. Atmos. Sci.,* **41,** 329–50.

Errico, R., and D. Baumhefner, 1987: Predictability experiments using a high-resolution limited area model. *Mon. Wea. Rev.*, **115**, 488–504.

Islam, S., 1991: Predictability of mesoscale precipitation. Sc.D. thesis, Department of Civil Engineering, Massachusetts Institute of Technology, Cambridge, 240 pp.

Jordan, C. L., 1958: Mean soundings for the West Indies area. *J. Meteorol.*, **15**, 91–97.

Leith, C. E., 1965: Numerical simulation of the Earth's atmosphere. *Methods in Computational Physics,* Academic Press, 1–28.

Lorenz, E. N., 1965: A study of predictability of a 28-variable atmospheric model. *Tellus,* **17**, 321–33.

——, 1982: Atmospheric predictability experiments with a large numerical model. *Tellus,* **34**, 505–13.

Mintz, Y., 1964: Very long term global integration of the primitive equations of atmospheric motions. *WMO-IUGG Symp. Res. Dev. Aspects of Long Range Forecasting,* World. Meteor. Org. Tech. Note No. **66,** 141–855.

Shukla, J., 1981: Dynamical predictability of monthly means. *J Atmos. Sci.*, **38**, 2547–2572.

Smagorinsky, J., 1969: Problems and promises of deterministic extended-range forecasting. *Bull. Amer. Meteor. Soc.*, **50**, 286–311.

Smolarkiewicz, P. K., and T. L. Clark, 1986: The multidimensional positive definite advection transport algorithm: Further development and applications. *J. Comp. Phys.,* **67**, 396–438.

Tennekes, H., 1978: Turbulent flow in two and three dimensions. *Bull. Amer. Meteor. Soc.,* **59**, 22–28.

Warner, T. T., and D. Keyser, 1983: Some practical insights into the relationship between initial state uncertainty and mesoscale predictability. *Proc. Conf. Predictability of Fluid Motions,* G. Holloway and B. J. West, Eds., La Jolla, California, American Institute of Physics, 271–286.

Xu, K., and K. A. Emanuel, 1989: Is the tropical atmosphere conditionally unstable? *Mon. Wea. Rev.,* **117**, 1471–1479.